Targeting the Surface of the Protein 14-3-3 by Ultrasmall (1.5 nm) Gold Nanoparticles Carrying the Specific Peptide CRaf

Tatjana Ruks,[a] Kateryna Loza,[a] Marc Heggen,[b] Christian Ottmann,[c] Peter Bayer,[d] Christine Beuck,[d] and Matthias Epple*[a]

The surface of ultrasmall gold nanoparticles with an average diameter of 1.55 nm was conjugated with a 14-3-3 protein-binding peptide derived from CRaf. Each particle carries 18 CRaf peptides, leading to an overall stoichiometry of Au(115)Craf(18). The binding to the protein 14-3-3 was probed by isothermal titration calorimetry (ITC) and fluorescence polarization spectroscopy (FP). The dissociation constant (K_D) was measured as 5.0 μM by ITC and 0.9 μM by FP, which was close to the affinity of dissolved CRaf to 14-3-3σ. In contrast to dissolved CRaf, which alone did not enter HeLa cells, CRAF-conjugated gold nanoparticles were well taken up by HeLa cells, opening the opportunity to target the protein inside a cell.

1. Introduction

The supramolecular interaction between small molecules and proteins is an important area in current biomedical research.[1] It opens the possibility to influence the function of proteins by specifically targeting surface epitopes. Peptides are especially useful as they give a highly selective interaction with proteins. The protein 14-3-3 is of special interest because it is one of the most widely connected "hub" proteins in humans,[2] therefore chemical agents that are targeting 14-3-3 protein-protein interactions (PPIs) are becoming increasingly interesting for drug discovery.[3] We have earlier shown that 14-3-3 PPIs can be modulated by natural products and their semisynthetic derivatives,[4] supramolecular ligands,[5] "classical" small molecules,[6] and fragments.[4d,7]

[a] Dr. T. Ruks, Dr. K. Loza, Prof. Dr. M. Epple
     Inorganic Chemistry and Center for Nanointegration Duisburg–Essen (CeNIDE)
     University of Duisburg-Essen
     Universitätsstrasse 5–7, 45117 Essen (Germany)
     E-mail: matthias.epple@uni-due.de
[b] Dr. M. Heggen
     Ernst Ruska-Centre for Microscopy and Spectroscopy with Electrons
     Forschungszentrum Jülich GmbH
     52425 Jülich (Germany)
[c] Prof. Dr. C. Ottmann
     Laboratory of Chemical Biology
     Department of Biomedical Engineering and
     Institute for Complex Molecular Systems (ICMS)
     Eindhoven University of Technology
     P.O. Box 513, 5600MB, Eindhoven (The Netherlands)
[d] Prof. Dr. P. Bayer, Dr. C. Beuck
     Department of Structural and Medicinal Biochemistry
     Centre for Medical Biotechnology (ZMB), University of Duisburg-Essen
     45117 Essen (Germany)

The potential of supramolecular binding molecules can be enhanced by conjugating them to an ultrasmall nanoparticle (1–2 nm). Such particles have a diameter even below the size of a protein. The possibility to attach more than one ligand to a single nanoparticle permits multiavid targeting of the protein surface.

Chemically, ultrasmall nanoparticles are at the borderline between atom-sharp metal clusters (ca. 1 nm) and "classical" metallic nanoparticles with a diameter of 10 nm or more. Due to their small size, they have been explored in the last years for biological and biomedical applications.[1d,8] For instance, such nanoparticles can serve as carriers of surface-conjugated cargo molecules into cells and (in some cases) even into the cell nucleus.[9] They can be surface-conjugated by thiol-containing ligands that lead to a strong Au–S covalent bond.[10] In the case of biomolecules, cysteine and cysteine-containing peptides and ligands are of particular value for nanoparticle conjugation.[9c–e,11]

The diphosphorylated (pS233pS259) CRaf peptide is a strong binder for 14-3-3 proteins.[1b,12] Here we demonstrate how ultrasmall gold nanoparticles can be surface-conjugated with the protein-targeting peptide CRaf (residues 229–264, subsequently termed as CRaf) and show their interaction with the protein 14-3-3σ and also their uptake by eukaryotic cells.

2. Results and Discussion

We have chosen the peptide CRaf in a cysteine-modified form for its conjugation to ultrasmall gold nanoparticles to target epitopes on the surface of the protein 14-3-3. Equidistant between the two phosphorylated residues pS233 and pS259, a cysteine was introduced at position 246, leaving the peptide binding arms unchanged. The peptide was attached to the ultrasmall gold nanoparticles via the thiol group of this cysteine.

ChemBioChem

Full Papers
doi.org/10.1002/cbic.202000761

Chemistry Europe
European Chemical
Societies Publishing

The size of the metallic nanoparticle core was probed by aberration-corrected transmission electron microscopy. It should be noted that the image contrast of the particles with respect to the background is weak, even with an aberration-corrected electron microscope, because of the small size of the particles with respect to the coating by a considerable amount of organic peptide shell (Figure 1) and the thickness of the carbon support. However, individual particles could be well distinguished with an average diameter of 1.55 nm. This corresponds to about 115 gold atoms under the assumption of a spherical particle.

The attachment of the CRaf peptide was shown by ^{1}H NMR spectroscopy (Figure 2). Clearly, the ligand was attached in unchanged form, with only small changes in the spectrum. This is due to the facts that the peptide is rather big, and that most amino acids (and protons) are in a considerable distance from the metal core and also likely retained most of their flexibility. Thus, peak broadening as it is usually observed with ligands on ultrasmall nanoparticles was mostly avoided.[11,13]

The peptide was firmly attached to the nanoparticles as demonstrated by ^{1}H DOSY NMR spectroscopy (Figure 3). Clearly, all ^{1}H NMR signals were associated with the same diffusion

Figure 3. Top: ^{1}H DOSY spectra of dissolved CRaf (left) and of CRaf-functionalized gold nanoparticles (right). Glycerol is an impurity from nanofiltration. Bottom: Stejskal-Tanner plots of dissolved CRaf (blue) and of CRaf-functionalized gold nanoparticles (red). The slope is proportional to the diffusion coefficient, indicating that nanoparticles diffuse more slowly and thus have a higher hydrodynamic diameter.
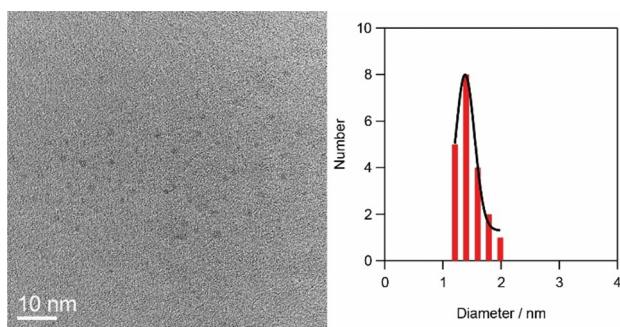

Figure 1. High-resolution transmission electron microscopy (HRTEM) of CRaf-conjugated ultrasmall gold nanoparticles. Left: particles. Right: particle size distribution.
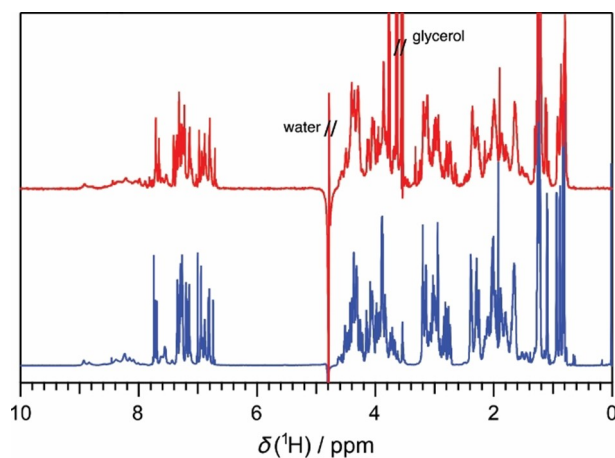
coefficient. As hydrodynamic diameter, 2.6 and 3.6 nm were obtained for peptide and nanoparticles, respectively. No free (unbound) CRaf was present in the nanoparticle dispersion.

The particle size distribution of the dispersed nanoparticles was also analyzed by differential centrifugal sedimentation (DCS), giving a hydrodynamic diameter of 1.5 nm (Figure 4). However, the diameters obtained by this method are systematically too small for functionalized ultrasmall nanoparticles because it is probing the hydrodynamic diameter by sedimentation, assuming a uniform density of the particle. Thus, this

Figure 2. ^{1}H NMR spectra of unlabeled CRaf in dissolved state (top) and attached to ultrasmall gold nanoparticles (bottom). Glycerol is an impurity from nanofiltration.
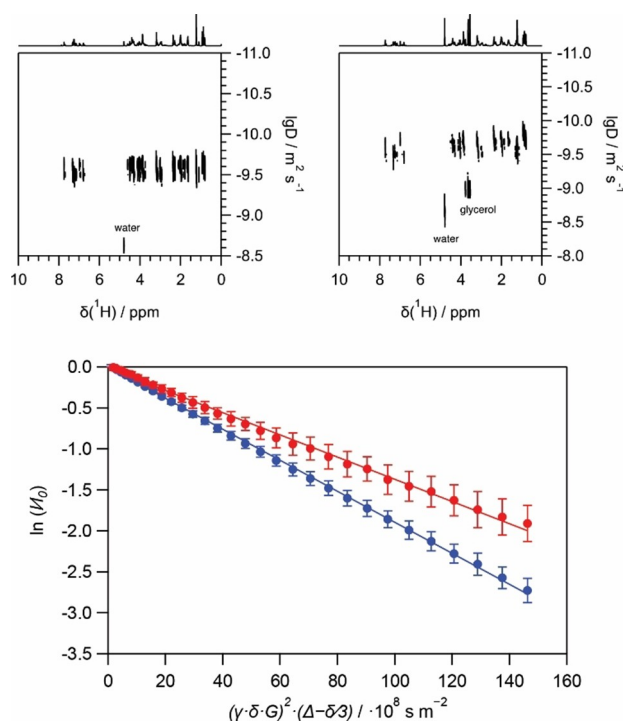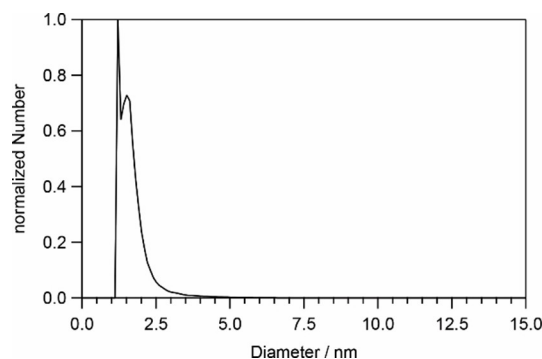

Figure 4. Differential centrifugal sedimentation of ultrasmall gold nanoparticles, functionalized with CRaf.

ChemBioChem

Full Papers
doi.org/10.1002/cbic.202000761

Chemistry Europe
European Chemical
Societies Publishing

diameter is clearly too small. If the solid particle carries a peptide shell, it sediments more slowly than expected because its effective density is lower than that of the gold core (19.3 g cm^{-3}).[14] Nevertheless, the DCS results clearly show that the nanoparticles are present in a well-dispersed state without major agglomerations. It is also noteworthy we worked at the borderline of the method with a centrifugation time of about 5 h, that is, the sedimentation rate was low due to the ultrasmall particle size. This is enhanced by the long peptide chain of CRaf that is attached to the nanoparticles, increasing the hydrodynamic diameter.

The surface loading of the nanoparticles with peptides was probed by UV spectroscopy with the FAM-labeled CRaf peptide (Figure 5). There was only little quenching (if at all) because the nanoparticles are ultrasmall, in accordance with earlier observations with similar nanoparticles.[9c] From the determination of the gold concentration by atomic absorption spectroscopy (AAS) which was converted to nanoparticles (1.55 nm, 115 gold atoms), we obtained 18 CRaf molecules on the surface of each gold particle (see the Experimental Section for a detailed calculation). As the molecular weight of each CRaf peptide is 4193 g mol^{-1}, the composition of each nanoparticle is about $115 \cdot 197$ g mol$^{-1} = 22\,655$ g mol^{-1} ($15\underline{5} \times 197 = 30\,535$) gold and $18 \cdot 4193$ g mol$^{-1} = 75\,474$ g mol^{-1} CRaf, giving a weight ratio of about $22\,655:75\,474 = 1:3.3 = m(\text{Au})/m(\text{CRaf})$. Consequently, each particle consists of about 23 wt% Au and 77 wt% peptide. In terms of volume, the metallic core (1.55 nm) occupies 1.95 nm^3, that is, only about 8% of the total hydrodynamic volume (24.4 nm^3, based on a hydrodynamic diameter of 3.6 nm). Each CRaf molecule has a molecular footprint of 0.41 nm^2. For cysteine on 1.78 nm gold nanoparticles, we found a smaller footprint of 0.15 nm$^{2[11]}$ which makes sense due to the bigger peptide CRaf and its "two-armed" attachment to the nanoparticle surface. Figure 6 visualizes the structure of a gold nanoparticle with a CRaf ligand, including its interaction with 14-3-3. The homodimeric protein 14-3-3σ has a molecular weight of 57.62 kDa and a diameter of about 6.8 nm (PDB ID: 4FJ3).[15]

The specific interaction of CRaf with 14-3-3σ was probed by isothermal titration calorimetry (Figure 7). The interaction of
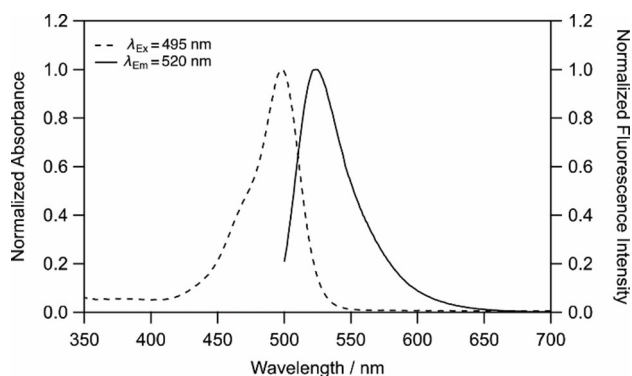
Figure 6. Top: Schematic view of the modified sequence of CRaf, conjugated to a gold nanoparticle (1.55 nm in diameter), visualized by PyMOL (The PyMOL Molecular Graphics System, Version 2.0 Schrödinger, LLC). Bottom: Schematic view of CRaf on a gold nanoparticle interacting with the homodimeric protein 14-3-3σ. Only the amino acids that interact with the protein binding region are shown; the other part of the chain is shown as a dashed line. The structural data were taken from the protein database (PDB ID: 4FJ3) and visualized by PyMOL.

Figure 7. Interaction of dissolved CRaf peptide with 14-3-3σ as probed by ITC. The differential heat flow (top) and the Wiseman plot (bottom) are shown.

Figure 5. Fluorescence excitation and emission spectra of FAM-labeled CRaf-functionalized ultrasmall gold nanoparticles with an absorption maximum at 495 nm and an emission maximum at 520 nm.
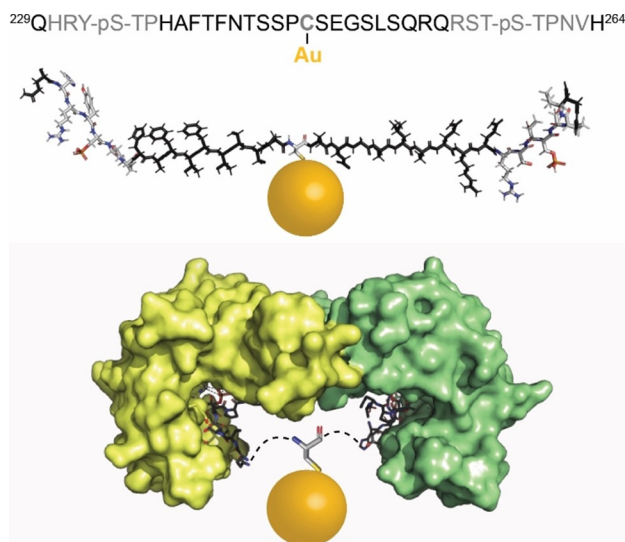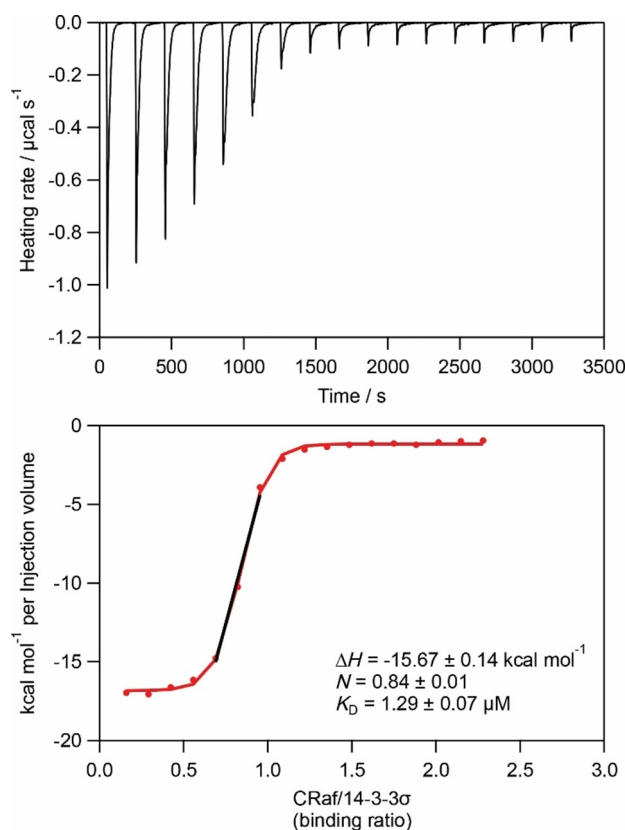
ChemBioChem

Full Papers
doi.org/10.1002/cbic.202000761

**Chemistry
Europe**
European Chemical
Societies Publishing

dissolved CRaf gave a dissociation constant K_D of 1.3 ± 0.1 μM, i.e. a rather strong interaction. The binding ratio CRaf/14-3-3σ was 0.84 ± 0.01, that is, each peptide was bound by one protein. The interaction was exothermic with 67 ± 1 kJ mol^{-1} (15.7 ±
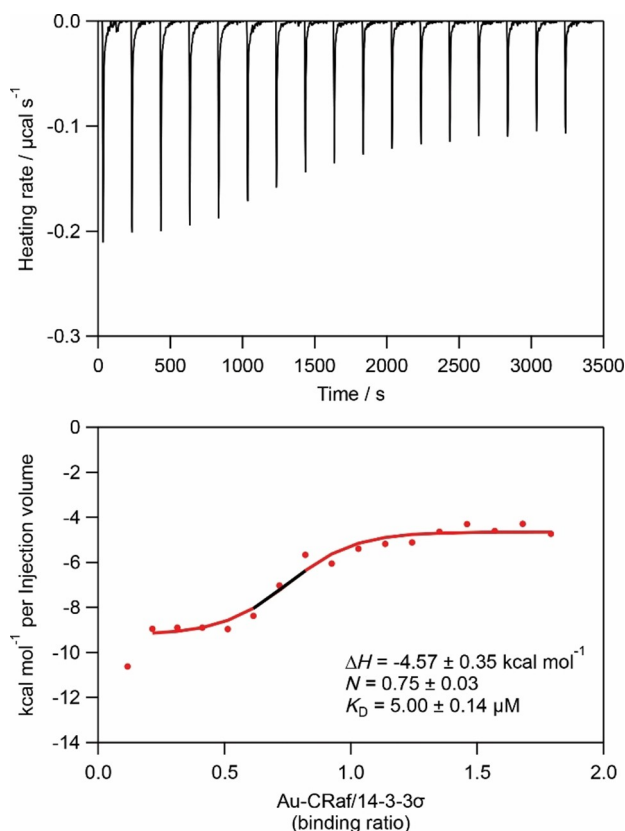

Figure 8. Interaction of CRaf-conjugated gold nanoparticles with 14-3-3σ as probed by ITC. The differential heat flow (top) and the Wiseman plot are shown with the concentration of CRaf set to 18 times the concentration of gold nanoparticles (bottom; see text).
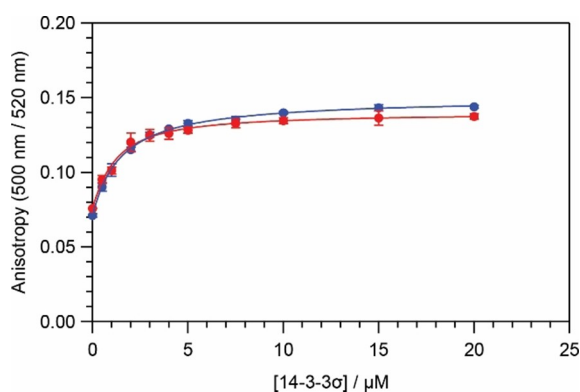

Figure 9. Interaction of dissolved FAM-CRaf and of FAM-CRaf-conjugated gold nanoparticles with 14-3-3σ as probed by FP. The starting concentration of dissolved FAM-CRaf was 20 nM ($V = 60$ μL). The starting concentration of the FAM-CRaf gold nanoparticles was 31 nM, corresponding to a peptide concentration of 560 nM ($V = 60$ μL). The concentration of the ligand CRaf was set to 18 times the gold nanoparticle concentration. The concentration of the added 14-3-3σ protein stock solution was 50 μM (total added volume 40 μL).

0.14 kcal mol^{-1}). However, the binding is weaker than reported earlier by Molzan et al. who found a K_D of 0.08 μM for CRaf and the isomer 14-3-3ζ.[16] This likely is an artifact of the fitting procedure because, in contrast to the free peptide in solution, not all peptides on a given nanoparticle can possibly be bound by protein due to steric reasons, which results in overestimating the K_D.

For nanoparticle-conjugated CRaf and 14-3-3σ, we measured a K_D of 5.0 ± 0.1 μM and a binding enthalpy of 19 ± 2 kJ mol^{-1} (4.57 ± 0.35 kcal mol^{-1}). The binding ratio CRaf/14-3-3σ dimer was 0.75 ± 0.03, that is, comparable to the free peptide (Figure 8).

Fluorescence polarization spectroscopy is an alternative method to study the interaction between a protein and a binding ligand. The protein 14-3-3σ was titrated to a solution of FAM-CRaf or a dispersion of FAM-CRaf on gold nanoparticles, respectively (Figure 9). For the dissolved ligand, we determined a K_D of 1.5 ± 0.1 μM, in good agreement with Molzan et al. for 14-3-3ζ.[16] For CRaf on gold nanoparticles, we found 0.9 ± 0.1 μM with 18 CRaf molecules on each gold nanoparticle. The binding strength was comparable or even slightly higher than that of CRaf alone.

For a practical application, it is important to target proteins inside cells. Therefore, we investigated the uptake of CRaf-conjugated gold nanoparticles by HeLa cells (Figure 10). The particles were easily taken up whereas dissolved CRaf could enter the cells only to a very small extent (Figure 11). This illustrates that a carrier is needed to transport functional peptides across the cell membrane. However, additional studies would be required to prove that the CRaf-functionalized nanoparticles are actually targeting the protein 14-3-3 inside the cell. The fact that we observed only few agglomerations by confocal microscopy indicates that the particles are well dispersed in cell culture medium. Unfortunately, dynamic light scattering is not applicable because the particles are too small.

Table 1 summarizes all measured properties of dissolved CRaf and of CRaf, conjugated to gold nanoparticles.
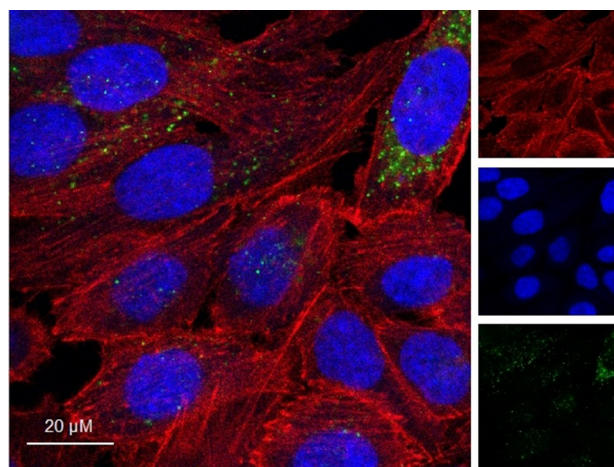

Figure 10. Uptake of FAM-CRaf-conjugated ultrasmall gold nanoparticles by HeLa cells (3.3·10^{14} nanoparticles per well; 10 000 cells per well) after 24 h of incubation. Actin: red, cell nucleus: blue, nanoparticles: green.
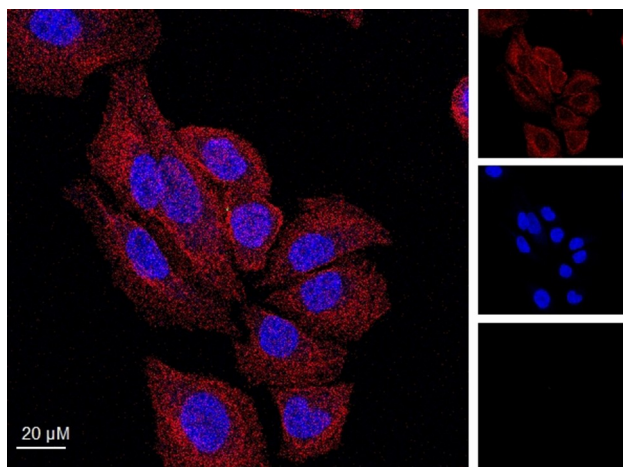
Figure 11. Uptake of FAM-CRaf by HeLa cells (CRaf concentration in the well 10 μM; 10000 cells per well) after 24 h of incubation. Actin: red, cell nucleus: blue, nanoparticles: green.

Table 1. Properties of dissolved CRaf and of CRAF-conjugated ultrasmall gold nanoparticles from ^{1}H DOSY, DCS, and HRTEM. An error of 10% for the diffusion coefficient and the hydrodynamic diameter measured by ^{1}H DOSY was assumed. Note that DCS systematically underestimates the particle diameter.

	Dissolved CRaf	Dispersed < Au-CRaf nanoparticles
$D(^1$H DOSY) [m^2 s^{-1}]	$(1.89 \pm 0.19) \times 10^{-10}$	$(1.36 \pm 0.14) \times 10^{-10}$
$d_h(^1$H DOSY) [nm]	2.6 ± 0.3	3.6 ± 0.4
d_h(DCS) [nm]	–	1.5 ± 0.5
d_{core}(HRTEM) [nm]	–	1.55 ± 0.24
K_D from ITC [μM]	1.3 ± 0.1	5.0 ± 0.1
binding ratio from ITC (peptide/protein)	0.84 ± 0.01	0.75 ± 0.03
binding enthalpy from ITC [kJ mol^{-1}]	66 ± 1	19 ± 2
K_D from FP [μM]	1.5 ± 0.1	0.9 ± 0.1
uptake by HeLa cells (24 h)	poor	good

3. Conclusions

The targeting of the relevant protein 14-3-3 is possible with peptide-functionalized ultrasmall gold nanoparticles. About 18 CRaf molecules can be covalently attached to a 1.55 nm ultrasmall gold nanoparticle. The binding ability of CRaf for 14-3-3σ remains unchanged as shown by isothermal titration calorimetry and fluorescence polarization spectroscopy. A particular advantage of the nanoparticles is their easy uptake by cells, opening up the possibility for protein targeting inside cells. This opens the pathway to target this protein inside cells with peptide-conjugated ultrasmall gold nanoparticles. The major advantage of ultrasmall nanoparticles is the fact that they are smaller than a protein. This makes them suitable to address epitopes on a protein, in contrast to larger "conventional" nanoparticles with a diameter of 10 nm or more. These are much larger than a protein. In that case the protein would target the nanoparticle instead of the nanoparticle targeting the protein. With such a specific attachment of the surface of a protein, its function during protein–protein interaction (PPi) should be controllable. This is demonstrated here for 14-3-3, but easily transposable to other proteins of biological or medical relevance. Future studies should address the selectivity of CRaf-functionalized nanoparticles by competitive binding studies in protein mixtures, ideally in living cells.

Experimental Section

Chemicals: An aqueous solution of tetrachloroauric(III)acid sodium salt (NaAuCl$_4$, prepared by dissolving sodium tetrachloroaurate(III) dihydrate (NaAuCl$_4 \cdot$ 2 H$_2$O, Sigma-Aldrich; 99%) in hydrochloric acid (37%) and ultrapure water) was used as gold source. Sodium borohydride (NaBH$_4$, Sigma-Aldrich; $\geq$ 96%) in aqueous solution was used as reducing agent. For the protein-interaction studies, the gold nanoparticles were conjugated either with the modified diphosphorylated CRaf peptide QHRY(pS) TPHAFTFNTSSP**C**SEGSLSQRQRST(pS)TPNVH-NH$_2$ (residues 229–264; 95–96%, 4192.63 g mol^{-1}), harboring a cysteine replacing serine 246 at the indicated site (mutant S246 C), or with its FAM-labeled derivate (5,6-FAM)-QHRY(pS)TPHAFTFNTSSP**C**SEGSLSQRQRST(pS) TPNVH-NH$_2$ (residues 229–264; 5,6-carboxyfluorescein fluorochrome conjugated to the C terminus; 97–98%, 4551.34 g mol^{-1}). It was important to minimize the formation of peptide disulfides during the synthesis (requiring work under inert gas atmosphere to avoid thiol oxidation) because disulfides are very difficult to remove from the nanoparticle dispersion after they have formed.

The peptides were obtained from Caslo ApS (Denmark) as lyophilized chloride salts and used as received without further purification. In all experiments, ultrapure water with a specific resistivity of 18.2 MΩ (Purelab ultra instrument from ELGA) was used as solvent unless otherwise stated. All glassware was cleaned with boiling *aqua regia* and ultrapure water before all reactions involving nanoparticles. The functionalized gold nanoparticles were stored in HEPES buffer (25 mM HEPES, 100 mM NaCl, 2 mM MgCl$_2$, 1 mM β-mercaptoethanol, pH 7.4) or in potassium phosphate buffer (47 mM K$_2$HPO$_4$ and 3 mM KH$_2$PO$_4$, pH 8) after the synthesis.

Nanoparticle synthesis: For the syntheses of peptide-functionalized gold nanoparticles, we dissolved 0.1–1.4 μmol peptide in 0.13–1.87 mL degassed water and adjusted the pH to 5.5–5.7 with 0.1 M sodium hydroxide solution. The amounts of NaAuCl$_4$ and NaBH$_4$ were adapted according to the molar amount of peptide. It was necessary to work at low pH to minimize the thiol oxidation to disulfide is difficult to remove.[17] Then, 1.4–19.5 μL NaAuCl$_4$ (corresponding to 33–467 nmol gold) was added to the peptide solution under stirring. The color of the peptide/gold mixture rapidly changed from yellow to colorless, indicating that the gold ions were reduced from Au^{+III} to Au^{+I}. After 10 min of cooling the mixture in an ice bath, 1–10 μL of 0.2 M NaBH$_4$ solution (freshly prepared with 4°C cold water; corresponding to 0.1–2 μmol) was added and stirred for another hour to reduce Au^{+I} to Au^0. We carried out all syntheses under inert gas atmosphere (argon, Schlenk technique).

The gold nanoparticles were purified by ultracentrifugation for 15 h at 30000 rpm (66,000 g). After that, we obtained two phases, that is, the dark brown concentrated gold nanoparticle dispersion in the lower part of the centrifugation tube and a colorless phase of unreacted parent compounds and synthesis by-products in the upper part. The colorless phase was carefully removed with a pipette. The nanoparticle dispersion was then purified by spin filtration with a Pierce^{TM} Protein Concentrator (PES, MWCO 10 kDA, 20 mL, Thermo Fisher) for 60 min at 4000 rpm (2000 g). Subsequently, the nanoparticles were multiply washed with HEPES buffer

ChemBioChem

Full Papers
doi.org/10.1002/cbic.202000761

**Chemistry
Europe**

European Chemical
Societies Publishing

or potassium phosphate buffer by redispersion/spin filtration. The resulting volume of the purified and concentrated nanoparticle dispersion was about 50 to 60 µL. The nanoparticle dispersion was light-brown. The absence of the typical red color due to surface plasmon resonance of larger gold nanoparticles (10 nm or more) confirms that all particles are ultrasmall-

Protein expression and purification: 14-3-3σ was expressed with a His$_6$-tag in NiCo21(DE3) competent cells from a pPRoeX-Htb vector in 2TY medium. The purification was carried out by affinity chromatography on nickel columns (HisTrap HP, 5 mL). The tags were cleaved with a TEV protease. The proteins were then loaded again on nickel columns to remove any uncleaved protein. A final purification step was performed by loading the proteins on a size-exclusion chromatography column (HiLoad 26/600 Superdex 75 pg) equilibrated in 20 mM TRIS-HCl buffer at pH 7.5, 150 mM NaCl, and 2 mM dithiothreitol (DTT). Before the ITC measurements, the protein was dialyzed with HEPES buffer (25 mM, pH 7.4).

Cell uptake studies: The uptake of peptide-functionalized ultra-small gold nanoparticles was carried out with human cervix carcinoma cells (HeLa). HeLa cells were cultured in Dulbecco's modified Eagle's medium (DMEM), supplemented with 10% fetal bovine serum (FBS), 100 U mL^{-1} penicillin, and 100 U mL^{-1} streptomycin at 37 °C in 5% CO$_2$ atmosphere. The cells were trypsinized and seeded in a glass-bottom dish (ibidi µ-Slide, Planegg, Germany) with 10^4 cells per well in 200 µL cell culture medium 24 h prior to the uptake studies. 20 µL of 125 µg mL^{-1} 5,6-FAM-CRaf-functionalized gold nanoparticles in 180 µL cell medium were added to the cells. The final gold nanoparticle concentration was 12.5 µg mL^{-1} per well, corresponding to 3.33·10^{14} nanoparticles per well. After incubation for 24 h, HeLa cells were washed 3 times with 200 µL phosphate-buffered saline (PBS) and fixed with 100 µL 4% aqueous paraformaldehyde (PFA) for 20 min at room temperature. The PFA was removed, and the cells were washed again three times with 200 µL PBS. For a better permeabilization of the dyes, the cells were treated with 150 µL of 0.1% Triton X-100 for 5 min and then washed twice with 200 µL PBS. Cell actin was stained by incubating the cells with 200 µL of 25 µg mL^{-1} Alexa-Fluor 660-phalloidin (Invitrogen) solution in PBS with 1% bovine serum albumin for 20 min. After washing the cells with PBS, the cells were incubated for 15 min with 150 µL of a 1 µg mL^{-1} solution of Hoechst33342 (Life Technologies) in PBS for nucleus staining. Afterwards, the cells were washed 3 times with PBS and then analyzed with a Leica TCS SP8 confocal laser scanning microscope with a 63 × NA1.2 water objective.

Analytical methods: The gold concentration in the nanoparticle dispersion was determined by atomic absorption spectroscopy (AAS) with a Thermo Electron M-Series spectrometer (graphite tube furnace according to DIN EN ISO/IEC 17025:2005) after dissolving the nanoparticles in aqua regia.

Analytical disc centrifugation (differential centrifugal sedimentation; DCS) was performed with a CPS Instruments DC 24000 disc centrifuge (24000 rpm). Two sucrose solutions (8 wt% and 24 wt%) formed a density gradient that was capped with 0.5 mL dodecane as stabilizing agent. The calibration standard was a poly(vinyl chloride) (PVC) latex in water with a particle size of 483 nm provided by CPS Instruments. A calibration was carried out prior to each run. A sample volume of 100 µL of dispersed nanoparticles was used. The recording time was about 6 h at the given centrifugation speed due to the small particle size. The density of elemental gold (19300 kg m^{-3}) was used for the computations.

UV/Vis spectroscopy was performed with a Varian Cary 300 instrument from 200 to 800 nm after background solvent correction

(HEPES buffer). Suprasil® quartz glass cuvettes with a sample volume of 500 µL were used.

Fluorescence spectroscopy was performed with an Agilent Technologies Cary Eclipse Spectrophotometer in the range of 500 to 700 nm after background solvent correction (HEPES buffer). A 96-well opaque flat bottom microplate with a sample volume of 300 µL was used.

High-resolution transmission electron microscopy was performed with an aberration-corrected FEI Titan transmission electron microscope equipped with a Cs-probe corrector (CEOS Company) and a point resolution of 0.08 nm operating at 300 kV.[18]

The nanoparticle concentrations were computed as follows (given here for a nanoparticle diameter of 1.55 nm and a gold concentration of 0.22 g L^1):

$$V_{NP} = \frac{4}{3} \cdot \pi \cdot \left(\frac{d}{2}\right)^3 = \frac{4}{3} \cdot 3.14 \cdot \left(\frac{1.55 \cdot 10^{-9}\ m}{2}\right)^3$$
$$= 1.95 \cdot 10^{-27}\ m^3$$

$$m_{NP} = V_{NP} \cdot \rho_{Au} = 1.95 \cdot 10^{-27}\ m^3 \cdot 19\ 302\ 000\ \frac{g}{m^3}$$
$$= 3.76 \cdot 10^{-20}\text{g}$$

$$c_{NP} = \frac{c_{Au}}{m_{NP}} = \frac{0.22\ \frac{g}{L}}{8.09 \cdot 10^{-20}g} = 5.85 \cdot 10^{18}\ L^{-1}$$

$$N_{NP} = c_{NP} \cdot V_{sample}$$

At a FAM-CRaf concentration of 179 µM as obtained by UV/Vis spectroscopy, this corresponds to 1.08×10^{20} FAM-Raf molecules per L, giving $1.08 \times 10^{20}/5.85 \times 10^{18} = 18$ FAM-CRaf molecules per gold nanoparticle.

NMR spectra were recorded in a 3 mm sample tube at 25 °C with a Bruker Avance III 700 MHz spectrometer, equipped with a 5 mm TCI ^{1}H/^{13}C/^{15}N/D cryoprobe with z-gradient. All gold nanoparticle dispersions and protein solutions were prepared in 200 µL in potassium phosphate buffer (47 mM K$_2$HPO$_4$ and 3 mM KH$_2$PO$_4$, pH 8) with 10% D$_2$O. The ^{1}H DOSY pulse program from the Bruker library was equipped with a presaturation pulse to suppress the water signal. For the DOSY experiments, a diffusion time Δ of 100 ms was used, and the pulsed gradient duration δ was 3 ms for the free peptide and 4 ms for the peptide conjugated to the gold nanoparticles. The gradient strength was incrementally increased from 5 to 95% of the maximum gradient strength (50.4 G cm^{-1} for a smoothed square gradient pulse) in 32 steps with a linear ramp to obtain a pseudo-2D DOSY data set. The spectra were Fourier-transformed, phased and integrated with the program versions 3.5 and 4.0.4 (Bruker). Plotting and fitting of the linearized diffusion data according to the Stejskal-Tanner equation[19]

$$\ln\left(\frac{I}{I_0}\right) = -\gamma^2 \delta^2 \left(\Delta - \frac{\delta}{3}\right) \cdot D \cdot G^2 \tag{1}$$

were performed with IGOR Pro (Wavemetrics, Inc.) with I as the signal intensity, I_0 as the signal intensity without gradient, γ as the gyromagnetic ratio of ^{1}H, δ as the diffusion gradient pulse length, Δ as the diffusion delay, G as the gradient strength, and D as the translational diffusion coefficient.

The Stejskal–Tanner plots of the well-discernible proton signals of the peptides and of the peptide-functionalized gold nanoparticles

ChemBioChem

Full Papers
doi.org/10.1002/cbic.202000761

Chemistry Europe
European Chemical
Societies Publishing

were first analyzed separately. Upon giving the same diffusion coefficient within the error margin, the relative intensities I/I_0 of all signals were averaged for dissolved peptide and nanoparticle-conjugated peptide, respectively. Error bars of the averaged data points represent the standard deviation of these proton signals. The accuracy of the diffusion coefficient was determined by averaging the errors obtained from the 2D ^{1}H DOSY spectrum.

The hydrodynamic diameter was calculated by the Stokes-Einstein equation

$$d_H = \frac{k \cdot T}{3\pi \cdot \eta \cdot D} \qquad (2)$$

with d_H the hydrodynamic diameter, k the Boltzmann constant, T the temperature [K], η the dynamic viscosity of H_2O at 25 °C, and D the translational diffusion coefficient.

Isothermal titration calorimetry (ITC) was performed with a Micro-CAL iTC2000 (Malvern Panalytical) instrument in HEPES buffer (25 mM, pH 7.4) at 25 °C. In the sample cell, 300 µL of 14-3-3σ (50 µM) was titrated with dissolved CRaf (1 mM), and 300 µL of 14-3-3σ (10 µM) was titrated with a dispersion of CRaf-functionalized gold nanoparticles (gold nanoparticle concentration 13.9 µM; CRaf concentration 0.25 mM), respectively. The first injection volume was 0.4 µL with a mixing time of 0.8 s and a time interval of 180 s. Then, 17 injections of 2 µL aliquots of the nanoparticle dispersion followed with a mixing time of 4 s and a time interval of 200 s, respectively. The measurements were carried out with an initial delay of 180 s, a reference power of 5 µcal s^{-1}, a stirring power of 750 rpm, and a filter period of 3 s. The dissociation constant ($K_D = 1/K_A$), the molar binding stoichiometry (N), and the molar binding enthalpy (ΔH^0) were calculated by integrating the peaks obtained from enthalpy changes and presenting them in a Wiseman plot.[20] A one-set-of-sites specific-binding model was assumed. The points 2 to 18 were fitted by the Hill Equation

$$H = H_0 + (H_{max} - H_0)\left(1 + \left(\frac{N}{n}\right)^{K_D}\right)^{-1} \qquad (3)$$

with H the molar enthalpy change per injection volume, H_0 the molar enthalpy change at the beginning of the measurement, H_{max} the maximum measured molar enthalpy change, n the molar ratio of peptide to protein, and N the molar binding stoichiometry. Here, the point of inflection gives the molar binding stoichiometry, and the slope at the point of inflection gives K_D. All data analyses were done with IGOR Pro.

Fluorescence polarization spectroscopy (FP) was performed with a JASCO FP-8300 fluorescence spectrometer in HEPES buffer (25 mM, pH 7.4) at 20 °C in Suprasil® quartz glass cuvettes with a sample volume of 60 µL. 14-3-3σ (50 µM) was added stepwise either to the FAM-labeled peptide (20 nM) or to the CRaf-functionalized gold nanoparticles (gold nanoparticle concentration 31 nM; CRaf concentration 560 nM). The resulting anisotropy at the emission wavelength of 520 nm was measured by exciting the sample with linearly polarized light at 500 nm. Fitting for the K_D determination was done with IGOR Pro with the following quadratic binding equation for a one-site specific binding model

$$r = r_0 + r_{max} \cdot \frac{([FL] + [[P] + K_D]) - \sqrt{([FL] + [P] + K_D)^2 - 4 \cdot [FL]}}{2 \cdot [FL]} \qquad (4)$$

with r the anisotropy, r_0 the anisotropy without protein, r_{max} the maximum anisotropy, [FL] the concentration of the titrant (fluorescently labeled CRaf), [P] the concentration of the added titrant (14-3-3σ), and K_D the dissociation constant.

Acknowledgements

Conflict of Interest

The authors declare no conflict of interest.

[1] a) F. Scaletti, J. Hardie, Y. W. Lee, D. C. Luther, M. Ray, V. M. Rotello, *Chem. Soc. Rev.* **2018**, *47*, 3421–3432; b) S. van Dun, C. Ottmann, L. G. Milroy, L. Brunsveld, *J. Am. Chem. Soc.* **2017**, *139*, 13960–13968; c) M. Kopp, S. Kollenda, M. Epple, *Acc. Chem. Res.* **2017**, *50*, 1383–1390; d) V. M. Rotello, *Beilstein J. Org. Chem.* **2016**, *12*, 1638–1646.

[2] a) N. N. Sluchanko, D. M. Bustos, *Prog. Mol. Biol. Transl. Sci.* **2019**, *166*, 19–61; b) M. Tinti, F. Madeira, G. Murugesan, G. Hoxhaj, R. Toth, C. Mackintosh, *Database (Oxford)* **2014**, *2014*, bat085.

[3] L. M. Stevers, E. Sijbesma, M. Botta, C. MacKintosh, T. Obsil, I. Landrieu, Y. Cau, A. J. Wilson, A. Karawajczyk, J. Eickhoff, J. Davis, M. Hann, G. O'Mahony, R. G. Doveston, L. Brunsveld, C. Ottmann, *J. Med. Chem.* **2018**, *61*, 3755–3778.

[4] a) L. M. Stevers, C. V. Lam, S. F. Leysen, F. A. Meijer, D. S. van Scheppingen, R. M. de Vries, G. W. Carlile, L. G. Milroy, D. Y. Thomas, L. Brunsveld, C. Ottmann, *Proc. Natl. Acad. Sci. USA* **2016**, *113*, E1152–1161; b) S. A. Andrei, P. de Vink, E. Sijbesma, L. Han, L. Brunsveld, N. Kato, C. Ottmann, Y. Higuchi, *Angew. Chem. Int. Ed. Engl.* **2018**, *57*, 13470–13474; c) A. Kaplan, S. A. Andrei, A. van Regteren Altena, T. Simas, S. L. Banerjee, N. Kato, N. Bisson, Y. Higuchi, C. Ottmann, A. E. Fournier, *Cell Chem. Biol.* **2020**, *27*, 657–667.e656; d) M. Wolter, P. de Vink, J. F. Neves, S. Srdanović, Y. Higuchi, N. Kato, A. Wilson, I. Landrieu, L. Brunsveld, C. Ottmann, *J. Am. Chem. Soc.* **2020**, *142*, 11772–11783.

[5] a) L. Bartsch, M. Bartel, A. Gigante, J. Iglesias-Fernández, Y. B. Ruiz-Blanco, C. Beuck, J. Briels, N. Toetsch, P. Bayer, E. Sanchez-Garcia, C. Ottmann, C. Schmuck, *ChemBioChem* **2019**, *20*, 2921–2926; b) D. Bier, S. Mittal, K. Bravo-Rodriguez, A. Sowislok, X. Guillory, J. Briels, C. Heid, M. Bartel, B. Wettig, L. Brunsveld, E. Sanchez-Garcia, T. Schrader, C. Ottmann, *J. Am. Chem. Soc.* **2017**, *139*, 16256–16263; c) D. Bier, R. Rose, K. Bravo-Rodriguez, M. Bartel, J. M. Ramirez-Anguita, S. Dutt, C. Wilch, F. G. Klärner, E. Sanchez-Garcia, T. Schrader, C. Ottmann, *Nat. Chem.* **2013**, *5*, 234–239; d) A. Gigante, J. N. Grad, J. Briels, M. Bartel, D. Hoffmann, C. Ottmann, C. Schmuck, *Chem. Commun.* **2018**, *55*, 111–114; e) A. Gigante, E. Sijbesma, P. A. Sánchez-Murcia, X. Hu, D. Bier, S. Bäcker, S. Knauer, F. Gago, C. Ottmann, C. Schmuck, *Angew. Chem. Int. Ed. Engl.* **2020**, *59*, 5284–5287.

[6] a) F. Bosica, S. A. Andrei, J. F. Neves, P. Brandt, A. Gunnarsson, I. Landrieu, C. Ottmann, G. O'Mahony, *Chem. Eur. J.* **2020**, *26*, 7131–7139; b) E. Sijbesma, E. Visser, K. Plitzko, P. Thiel, L. G. Milroy, M. Kaiser, L. Brunsveld, C. Ottmann, *Nat. Commun.* **2020**, *11*, 3954.

[7] a) X. Guillory, M. Wolter, S. Leysen, J. F. Neves, A. Kuusk, S. Genet, B. Somsen, J. K. Morrow, E. Rivers, L. van Beek, J. Patel, R. Goodnow, H. Schoenherr, N. Fuller, Q. Cao, R. G. Doveston, L. Brunsveld, M. R. Arkin, P. Castaldi, H. Boyd, I. Landrieu, H. Chen, C. Ottmann, *J. Med. Chem.* **2020**, *63*, 6694–6707; b) E. Sijbesma, K. K. Hallenbeck, S. Leysen, P. J. de Vink, L. Skóra, W. Jahnke, L. Brunsveld, M. R. Arkin, C. Ottmann, *J. Am. Chem. Soc.* **2019**, *141*, 3524–3531.

[8] a) L. Shang, S. J. Dong, G. U. Nienhaus, *Nano Today* **2011**, *6*, 401–418; b) A. Leifert, Y. Pan-Bartnek, U. Simon, W. Jahnen-Dechent, *Nanoscale* **2013**, *5*, 6224–6242; c) R. C. Jin, K. Nobusada, *Nano Res.* **2014**, *7*, 285–300; d) N. H. Kim, M. J. Hackett, J. Park, T. Hyeon, *Chem. Mater.* **2014**, *26*, 59–71; e) Z. Luo, K. Zheng, J. Xie, *Chem. Commun.* **2014**, *50*, 5143–5155; f) K. Y. Zheng, X. Yuan, N. Goswami, Q. B. Zhang, J. P. Xie, *RSC Adv.* **2014**, *4*, 60581–60596; g) A. M. Smith, L. E. Marbella, K. A. Johnston, M. J. Hartmann, S. E. Crawford, L. M. Kozycz, D. S. Seferos, J. E. Millstone, *Anal. Chem.* **2015**, *87*, 2771–2778; h) X. Zhang, S. Shastry, S. E. Bradforth, J. L. Nadeau, *Nanoscale* **2015**, *7*, 240–251; i) K. Zarschler, L. Rocks, N. Licciardello, L. Boselli, E. Polo, K. P. Garcia, L. De Cola, H. Stephan, K. A. Dawson, *Nanomedicine* **2016**, *12*, 1663–1701; j) S. Kenzler, C. Schrenk, A. R. Frojd, H. Hakkinen, A. Z. Clayborne, A. Schnepf, *Chem. Commun.* **2018**, *54*, 248–251; k) C. J. Zeng, *Pure Appl. Chem.* **2018**, *90*, 1409–1427; l) R. S. Ferreira, A. L. Lira, R. J. S. Torquato, P. Schuck, A. A. Sousa, *J. Phys. Chem. C* **2019**, *123*, 28450–28459; m) K. Kwak, D. Lee, *Acc. Chem. Res.* **2019**, *52*, 12–22; n) M. C. Bowman, T. E. Ballard, C. J. Ackerson, D. L. Feldheim, D. M. Margolis, C. Melander, *J. Am. Chem. Soc.* **2008**, *130*, 6896–6897; o) S. Jha, F. Ramadori, S. Quarta, A. Biasiolo, E. Fabris, P. Baldan, G. Guarino, M. Ruvoletto, G. Villano, C. Turato, A. Gatta, F. Mancin, P. Pontisso, P. Scrimin, *Bioconjugate Chem.* **2017**, *28*, 222–229; p) L. L. Knittel, H. Zhao, A. Nguyen, A. Miranda, P. Schuck, A. A. Sousa, *J. Phys. Chem. B* **2020**, *124*, 3892–3902; q) S. A. Miller, L. A. Hiatt, R. G. Keil, D. W. Wright, D. E. Cliffel, *Anal. Bioanal. Chem.* **2011**, *399*, 1021–1029; r) A. A. Sousa, S. A. Hassan, L. L. Knittel, A. Balbo, M. A. Aronova, P. H. Brown, P. Schuck, R. D. Leapman, *Nanoscale* **2016**, *8*, 6577–6588.

[9] a) S. Huo, S. Jin, X. Ma, X. Xue, K. Yang, A. Kumar, P. C. Wang, J. Zhang, Z. Hu, X. J. Liang, *ACS Nano* **2014**, *8*, 5852–5862; b) K. Y. J. Lee, G. Y. Lee, L. A. Lane, B. Li, J. Q. Wang, Q. Lu, Y. Q. Wang, S. M. Nie, *Bioconjugate Chem.* **2017**, *28*, 244–252; c) S. B. van der Meer, K. Loza, K. Wey, M. Heggen, C. Beuck, P. Bayer, M. Epple, *Langmuir* **2019**, *35*, 7191–7204; d) V. Sokolova, G. Nzou, S. B. van der Meer, T. Ruks, M. Heggen, K. Loza, N. Hagemann, F. Murke, B. Giebel, D. M. Hermann, A. J. Atala, M. Epple, *Acta Biomater.* **2020**, *111*, 349–362; e) V. Sokolova, G. Mekky, S. B. van der Meer, M. C. Seeds, A. J. Atala, M. Epple, *Sci. Rep.* **2020**, *10*, 18033.

[10] H. Häkkinen, *Nat. Chem.* **2012**, *4*, 443–455.

[11] T. Ruks, C. Beuck, T. Schaller, F. Niemeyer, M. Zähres, K. Loza, M. Heggen, U. Hagemann, C. Mayer, P. Bayer, M. Epple, *Langmuir* **2019**, *35*, 767–778.

[12] M. Molzan, B. Schumacher, C. Ottmann, A. Baljuls, L. Polzien, M. Weyand, P. Thiel, R. Rose, M. Rose, P. Kuhenne, M. Kaiser, U. R. Rapp, J. Kuhlmann, C. Ottmann, *Mol. Cell. Biol.* **2010**, *30*, 4698–4711.

[13] a) G. Salassa, T. Burgi, *Nanoscale Horiz.* **2018**, *3*, 8; b) C. Guo, J. L. Yarger, *Magn. Reson. Chem.* **2018**, *56*, 1074–1082.

[14] H. Fissan, H. Kaminski, C. Asbach, M. Epple, *Anal. Methods* **2014**, *6*, 7324–7334.

[15] M. Molzan, C. Ottmann, *J. Mol. Biol.* **2012**, *423*, 486–495.

[16] M. Molzan, S. Kasper, L. Roglin, M. Skwarczynska, T. Sassa, T. Inoue, F. Breitenbuecher, J. Ohkanda, N. Kato, M. Schuler, C. Ottmann, *ACS Chem. Biol.* **2013**, *8*, 1869–1875.

[17] a) L. B. Poole, *Free Radical Biol. Med.* **2015**, *80*, 148–157; b) J. P. Tam, C. R. Wu, W. Liu, J. W. Zhang, *J. Am. Chem. Soc.* **1991**, *113*, 6657–6662.

[18] A. Thust, J. Barthel, K. Tillmann, *J. Large-Scale Res. Fac.* **2016**, *2*, A41.

[19] a) A. S. Altieri, D. P. Hinton, R. A. Byrd, *J. Am. Chem. Soc.* **1995**, *117*, 7566–7567; b) E. O. Stejskal, J. E. Tanner, *J. Chem. Phys.* **1965**, *42*, 288.

[20] T. Wiseman, S. Williston, J. F. Brandts, L. N. Lin, *Anal. Biochem.* **1989**, *179*, 131–137.